Supporting Information

Roberts et al. 10.1073/pnas.1511252113

Assumption of Zonal Continuity Across the Sub-Antarctic South Atlantic

Developing an understanding of changes in the physical properties of seawater with depth typically requires depth transect of sediment cores that are located within a confined region, where surface signals should be common to all sites. However, due to a lack of available cores from intermediate water depths in the Eastern Atlantic/Cape Basin combined with low sedimentation rates at those few sites (e.g., refs. 11, 52, 53) and the dearth of deep sites in the Western sub-Antarctic Atlantic, it was necessary to study two rather distal sites (Fig. S1). Despite the geographic separation of these cores, they underlie roughly equivalent surface circumpolar ocean regimes (Sub-Antarctic Zone). The modern sub-Antarctic Atlantic is zonally continuous, in terms of potential density (Fig. S1). In this study we make the assumption that deglacial changes occurring at either site would occur everywhere synchronously in water at the same depth in the sub-Antarctic South Atlantic. We acknowledge that for our findings from the South Atlantic to have global implications, further studies, particularly from the Pacific sector, are required.

Age Model (GC528)

The age model for GC528 was generated using 25 radiocarbon dates of monospecific samples of *U. bifurcata* (*Methods*). The age markers of GC528 are tabulated in Table S1.

Carbon-14 ages were calibrated using Bacon age-modeling software (43) with the Marine13 dataset (44) (Table S1 and Fig. S2). The age model suggests highly variable sedimentation rates in the core across the last deglaciation from ∼10 cm/ky in the Holocene to ∼40 cm/ky at the LGM. The high mean sedimentation rates during the glacial period can be explained by a decrease in sea level which acts to bring the coastline, the source of terrigenous material, closer to the core site.

Uvigerina spp. Cleaning

In addition to the Mg/Ca data generated in this study, further Mg/Ca data from MD07-3076Q was used which had been cleaned using a different approach. This additional *Uvigerina* spp. Mg/Ca data was cleaned using the clay removal and silicate removal steps (45), but without a full oxidative cleaning. Comparison of samples which had been both oxidatively cleaned and nonoxidatively cleaned show an average offset of 0.045 mmol/mol (Fig. S3). We corrected the nonoxidatively cleaned samples by –0.045 mmol/mol; however, this does not significantly change the overall temperature trend (Fig. S3).

Mn/Ca was measured to monitor cleaning efficiency and diagenetic effects. There is no relationship between Mn/Ca and Mg/Ca (Fig. S4), implying that diagenetic coatings are not affecting the Mg/Ca ratio. Nonoxidatively cleaned samples typically have a higher Mn/Ca ratio than oxidatively cleaned samples; however, the concentration of Mn/Ca is so small (up to 0.3 mmol/mol) that the Mg contribution of a diagenetic coating would have minimal effect. A Mg/Mn ratio of 0.1 mol/mol within a diagenetic coating, consistent with Mg/Mn ratios found in manganese carbonate in marine sediments (54), would imply a maximum contribution of 10^{-2} mmol/mol to Mg/Ca in this record, well within the reproducibility found from duplicate analyses.

Mg/Ca-Temperature Calibration

Comparison of available *Uvigerina* spp. Mg/Ca-temperature calibrations in the literature shows there is a considerable range in the regression lines (Fig. S5). We find that the best-fit calibration curve to the core top data from GC528 and MD07-3076Q is provided by the core-top calibration study of Elderfield et al. (18). However, we find that this calibration generates temperature estimates below the freezing point of seawater for GC528 at the LGM, the minimum temperature being –3.8 °C. This may be in part caused by the lack of Mg/Ca core-top constraints for bottom water below 0 °C. We attempt to improve the calibration by adding the constraint that the LGM minimum Mg/Ca value in GC528 measured cannot record temperature below the freezing point of seawater (Fig. S5). The new calibration curve is defined as

$$\mathrm{Mg/Ca} = (0.0915 \pm 0.005) * \mathrm{T} + (0.843 \pm 0.035) \quad R^2 = 0.92.$$

The 1σ uncertainty in the temperature estimate of each sample is ±0.7 °C. Discussion of the propagation of error in benthic temperatures can be found below.

However, it is important to note that the choice of calibration line does not alter our main observation of a decrease in the density gradient over the deglacial period (Fig. S6).

Subtracting the Global Ice Volume Effect

To calculate salinity, the isotopic effect of melting continental ice must be subtracted from the $\delta^{18}O$ of seawater (as calculated from the paleotemperature equation) to apply modern salinity–δw relationships. The ice volume effect was calculated assuming a linear relationship (21) between sea level (19) and $\delta^{18}O$ of seawater. The isotopic effect of melting ice will have spatial and temporal variations which are masked in our subtraction of a global mean δ_w, but these remain poorly constrained. As transient $\delta^{18}O$ tracer models that provide information on local $\delta^{18}O$ variability and their governing mechanisms are not available, we adhere to the global mean isotopic $\delta^{18}O$ record as the best approximation for ice sheet melt derived changes in ocean δ_w. The effect of subtracting the global ice volume effect from the calculated $\delta^{18}O$ of seawater is shown in Fig. S7.

Choice of Regression Line Between Salinity and $\delta_{w\text{-}ice}$

In this study we use the modern Southern Ocean linear relationship between salinity and $\delta_{w\text{-}ice}$ (21)and assume that it holds across the deglacial period. We argue that processes such as brine rejection may have the effect of increasing salinity without increasing $\delta_{w\text{-}ice}$, thus the salinity estimates should be considered minimum salinity estimates.

An alternative regression line may be based on the LGM salinity and seawater $\delta^{18}O$ estimates of Adkins et al. (15) from the two Southern Ocean sites, 1123 and 1093. Assuming 1‰ of the LGM seawater $\delta^{18}O$ is related to the ice volume, the regression line between salinity and $\delta_{w\text{-}ice}$ based on the pore-water studies is

$$\delta_{w\text{-}ice} = 0.191 * \mathrm{S} - 6.913.$$

The difference between the salinity estimates produced by this "LGM regression line" and the "modern Southern Ocean regression line" used in the paper is small relative to the magnitude of the change in salinity over the deglaciation (Fig. S8). We have chosen the modern Southern Ocean regression line over the LGM regression line based on the fact that it has more data making up the regression and the data included in the regression are located within the region of MD07-3076Q and GC528.

In this study we make the assumption that the relationship between salinity and $\delta_{w\text{-}ice}$ does not significantly differ between the Holocene and the LGM. There are a couple of lines of evidence which can be used to justify this assumption. First, we have

performed a simple thought experiment whereby we pose the question: What must the salinity–$\delta_{w\text{-}ice}$ relationship have to be at the LGM to eradicate the late deglacial decrease in salinity? We find that the required salinity–$\delta_{w\text{-}ice}$ relationship plots well outside the range of modern southern hemisphere water masses and well outside the predicted LGM salinity–$\delta_{w\text{-}ice}$ relationship from pore-water profiles (15) (Fig. S9), provided the reported pore-water–derived LGM salinity and δ_w estimates are robust (24). We therefore suggest that it is valid to invoke significant seawater salinity variations to explain the observed $\delta_{w\text{-}ice}$ change in MD07-3076Q. A second line of evidence supporting the idea that a change in the salinity–$\delta_{w\text{-}ice}$ relationship did not occur over the last deglaciation comes from newly published isotope-enabled GCM studies (22). This study found that the South Atlantic exhibits a relatively constant salinity–$\delta_{w\text{-}ice}$ relationship across spatial and temporal scales supporting the validity of applying a temporally constant salinity–$\delta_{w\text{-}ice}$ relationship to our datasets.

Propagation of Errors in the Conversion of Mg/Ca to Benthic Temperature

Propagating the replicate error ($\sigma_{Mg/Ca} = 0.7$ °C) and the error in the new calibration curve ($\sigma_{calib} = 1.1$ °C) gives a 1σ uncertainty in the temperature estimate of each sample of ±1.3 °C. Previously published calibrations typically give 1σ uncertainties of 0.5–1.0 °C (e.g., ref. 55). This difference may be due to a less critical assessment of the errors involved in the calibration curve.

However, the errors associated with the calibration curve (σ_{calib}) are largely due to it being based on old data from different laboratories, with different cleaning procedures. It is likely that improvements in analytical technique have decreased the error associated with the calibration curve. The data used in this study were generated in the same laboratory, using the same method and have been checked for repeatability. We infer that although the absolute values for temperature may be uncertain, the raw Mg/Ca values generated in each core should be directly comparable. Therefore, we assume an error in benthic temperatures of 0.7 °C, equivalent to the replicate error in the Mg/Ca measurement.

Propagation of Errors in the Calculation of Potential Density

To calculate in situ density at each site, salinity had to be calculated, which was derived from the ice-volume corrected $\delta^{18}O$ of seawater ($\delta_{w\text{-}ice}$).

Using the paleotemperature equation (20), the $\delta^{18}O$ of seawater (δ_w) is calculated. The error in the $\delta^{18}O$ of seawater ($\sigma_{\delta w}$) is a combination of the error in the measurement of $\delta^{18}O$ of *Uvigerina* spp. ($\sigma_{\delta c} = 0.08‰$) and the error in the Mg/Ca-derived benthic temperature ($\sigma_T = 0.18‰$): $\sigma_{\delta w}{}^2 = \sqrt{\sigma_T{}^2 + \sigma_{\delta c}{}^2}$, consequently $\sigma_{\delta w} = 0.19‰$.

To compare paleoestimates of $\sigma_{\delta w}$ with modern data, the so-called "ice volume effect" is removed. Using a compilation of observed sea-level estimates (19), we calculate the isotopic effect from the melting of continental ice and estimate a variance of $\sigma_{SL} = 0.10‰$. This gives a total error in the ice-volume–corrected $\delta^{18}O$ of seawater of $\sigma_{\delta w\text{-}ice} = \sqrt{\sigma_{\delta w}{}^2 + \sigma_{SL}{}^2} = 0.22‰$.

We assume a linear relationship between $\sigma_{\delta w\text{-}ice}$ and salinity, based on the Southern Ocean gridded $\delta^{18}O$ seawater data set (21). The variance in salinity σ_S is calculated using the σ_{slope} and σ_{icept} given in ref. 21:

$$\sigma_S = \sqrt{\sigma_{\delta w}^2\left(\frac{\partial \delta w}{\partial S}\right)^2 + \sigma_{icept}^2\left(\frac{\partial \delta icept}{\partial S}\right)^2 + \sigma_{slope}^2\left(\frac{\partial slope}{\partial S}\right)^2} = 2.24 \text{ psu.} \quad \textbf{[S1]}$$

In situ density was calculated using the equation of state expressed in ref. 23. Variance was calculated similarly to Eq. **S1**, returning a variance in in situ density of $\sigma_\theta = 1.85$ kg/m^3.

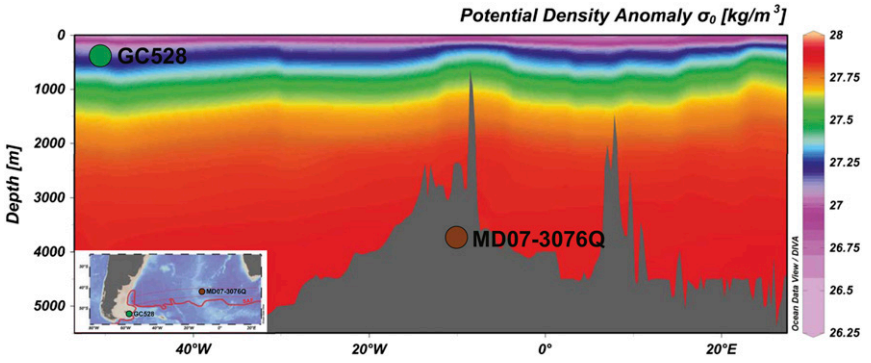

Fig. S1. Density transect of Southern Ocean along the Sub-Antarctic Front (WOA09_Annual). There is minimal zonal difference in density between the eastern and western Atlantic basins. In this study we assume that this zonal continuity remains over the deglaciation, and use the cores to reconstruct a depth transect of the Southern Ocean.

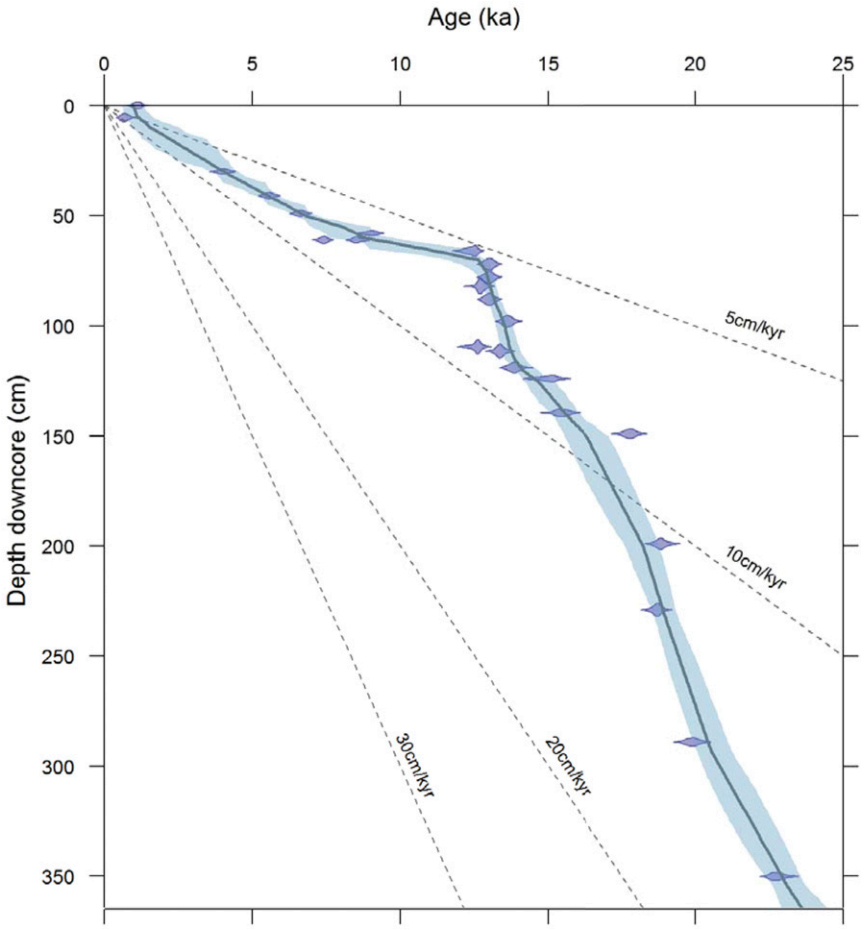

Fig. S2. GC528 age model based on 25 radiocarbon dates on the benthic foraminifera *U. bifurcata*. Output age model generated using the Bayesian age-depth modeling software Bacon (43).

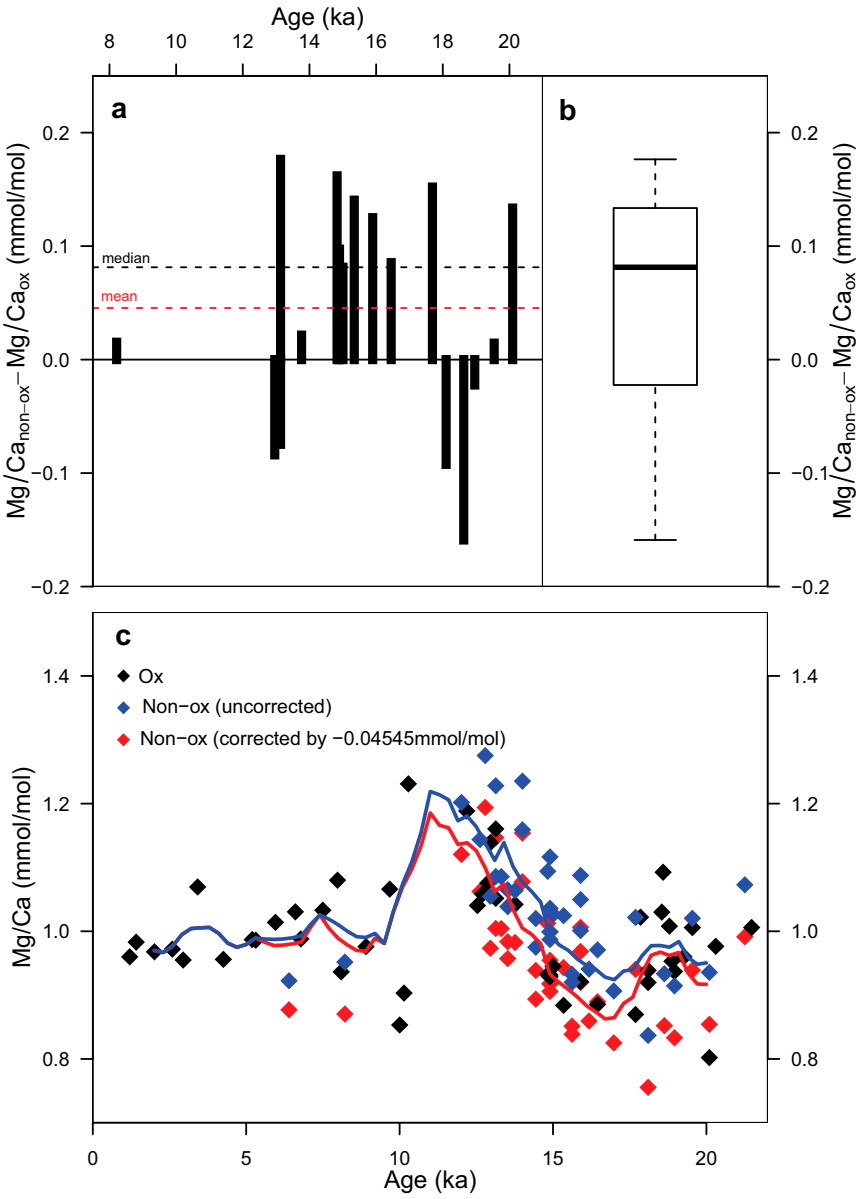

Fig. S3. Comparison of oxidatively cleaned samples versus nonoxidatively cleaned samples. (*A*) Difference in Mg/Ca ratio between samples from the same depth interval cleaned nonoxidatively and samples cleaned oxidatively. (*B*) Barplot summarizing the distribution in *A*. (*C*) Timeseries showing the difference in the Mg/Ca values of oxidatively cleaned samples (black) compared with nonoxidative samples (blue) and nonoxidative samples corrected by −0.045 mmol/mol (red).

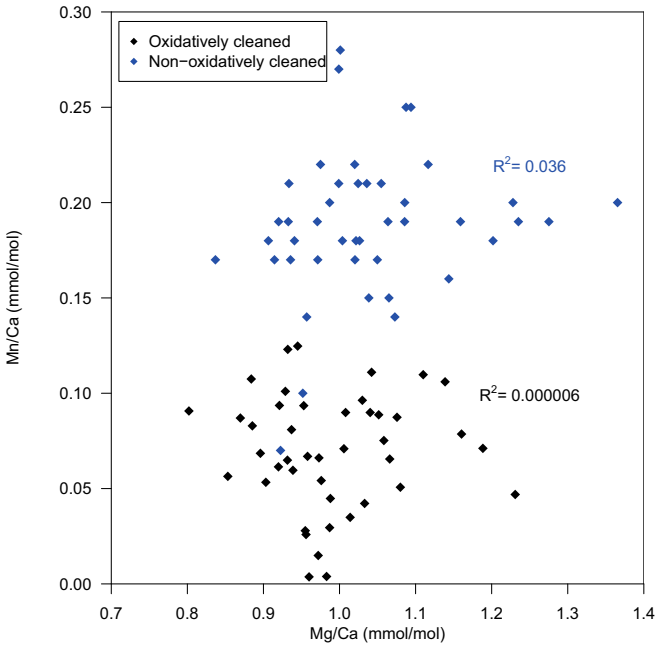

Fig. S4. Cross-plot of Mn/Ca versus Mg/Ca for MD07-3076Q. There is no correlation between Mn/Ca and Mg/Ca for either oxidatively cleaned (black) or nonoxidatively cleaned samples (blue) suggesting that diagenetic coatings do not affect the Mg/Ca measured.

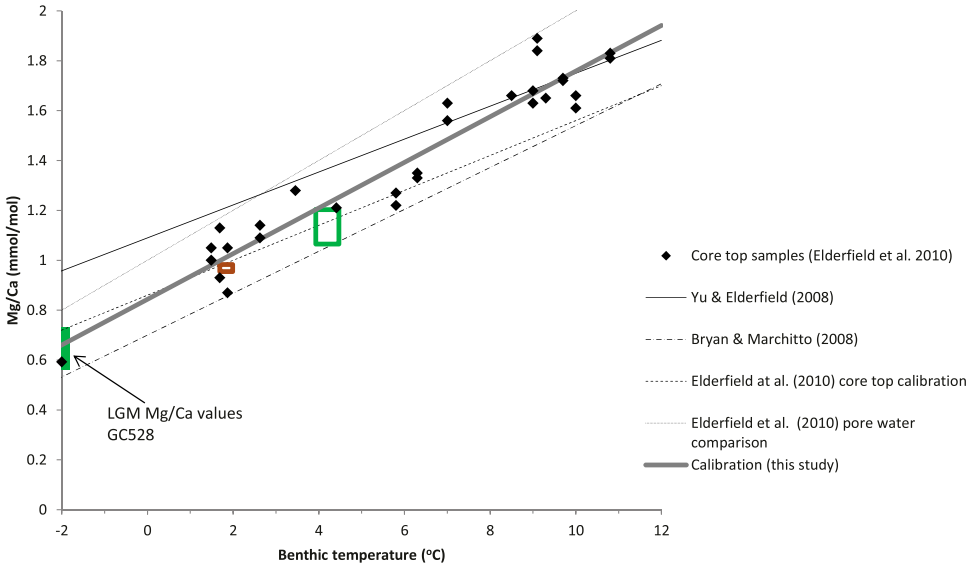

Fig. S5. Comparison of published *Uvigerina* spp. calibration curves. Comparison of various *Uvigerina* spp. Mg/Ca-temperature calibration curves: Bryan and Marchitto (56), dot-dashed line; Yu and Elderfield (57), solid line; Elderfield et al. (18) core-top calibration, dashed line; Elderfield et al. (18) pore-water calibration, dotted line. The low-temperature core-top data from Elderfield et al. (18) are displayed as black diamonds. The Mg/Ca data from the top of the two cores are plotted as green (GC528) and brown (MD07-3076Q) boxes. Calibration of Mg/Ca-benthic temperatures based on data from Elderfield et al. (18) has been improved with an additional constraint that the minimum Mg/Ca value (green bar on the *y* axis) cannot generate a benthic temperature below the freezing point of seawater. This amended calibration is shown as a bold gray line.

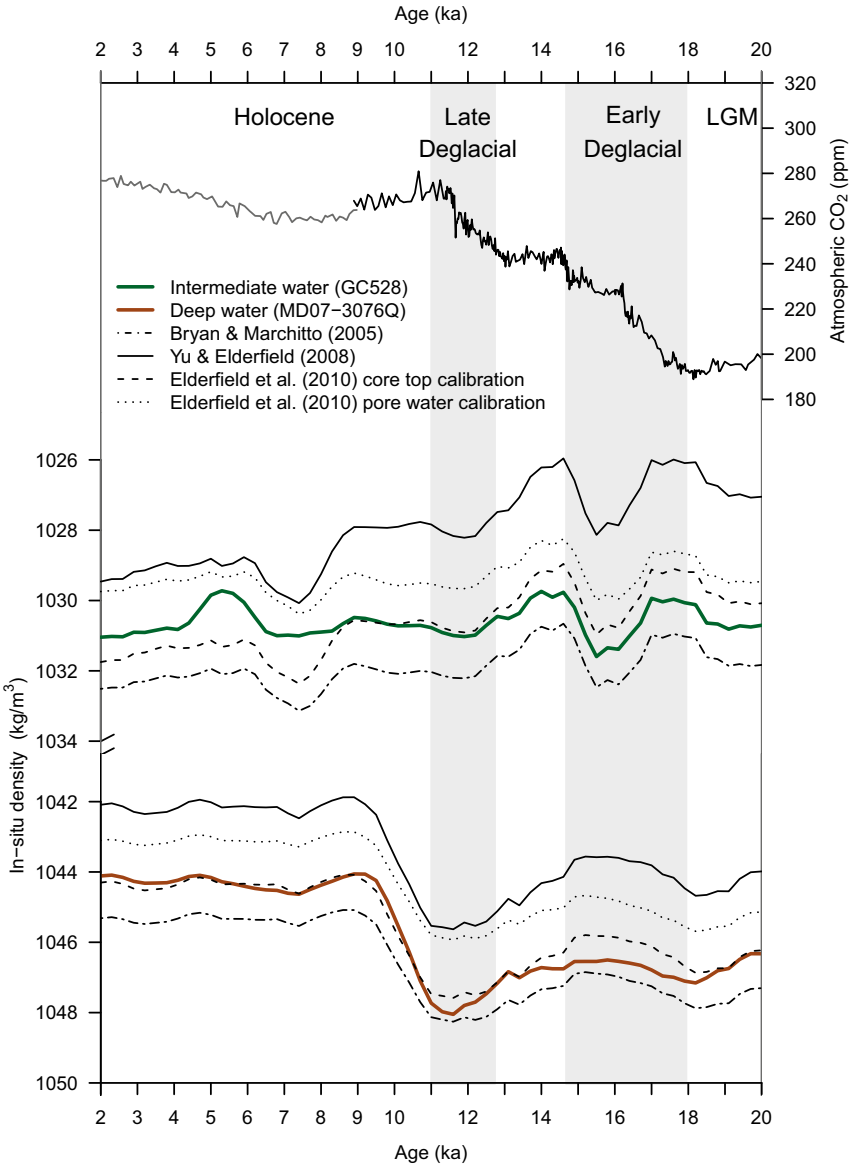

Fig. S6. Comparison of in situ density of GC528 and MD07-3076Q based on different calibration curves. Comparison of the in situ density of generated using various *Uvigerina* spp. Mg/Ca-temperature calibration curves: Bryan and Marchitto (56), dot-dashed line; Yu and Elderfield (57), solid line; Elderfield et al. (18) core-top calibration, dashed line; Elderfield et al. (18) pore-water calibration, dotted line. Mg/Ca-temperature calibration used in this study shown by the green and brown lines.

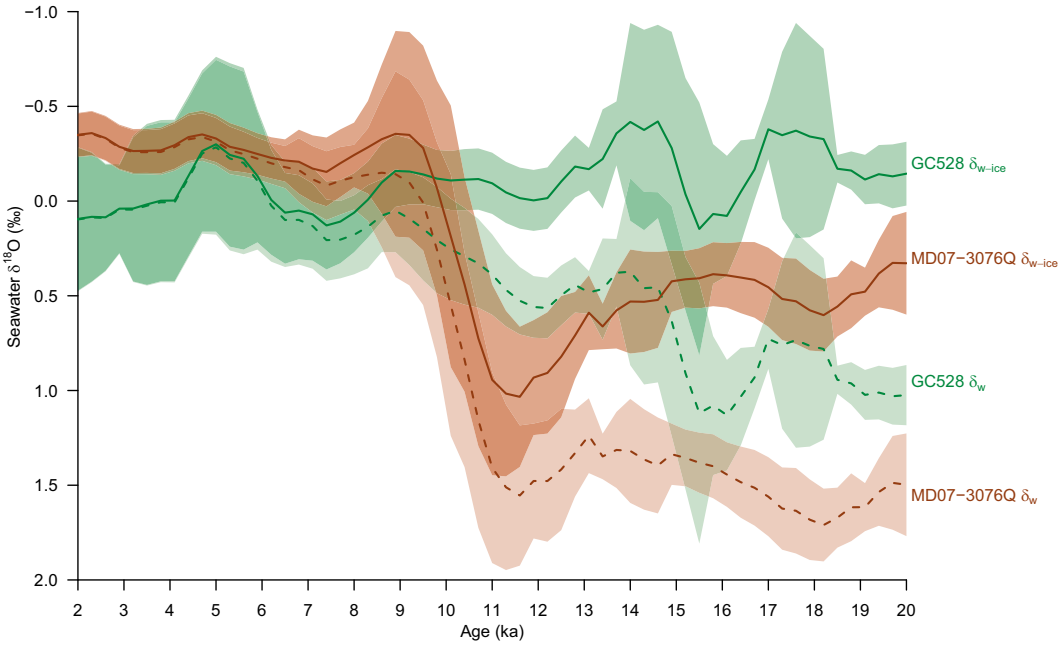

Fig. S7. Comparison of seawater $\delta^{18}O$ before (dashed) and after (solid) ice volume correction.

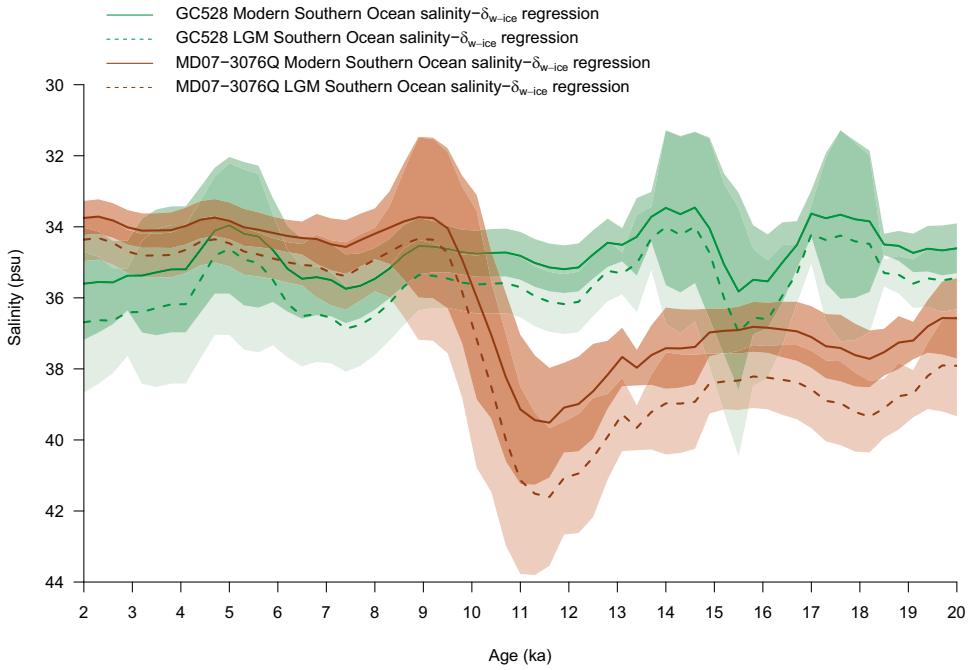

Fig. S8. Comparison of salinity estimates based on different salinity–$\delta_{w\text{-}ice}$ regression lines. "Modern regression" is based on the modern salinity–$\delta_{w\text{-}ice}$ relationship for the Southern Ocean (21). "LGM regression" uses LGM pore-water salinity and $\delta_{w\text{-}ice}$ estimates from site 1123 and 1093 (15).

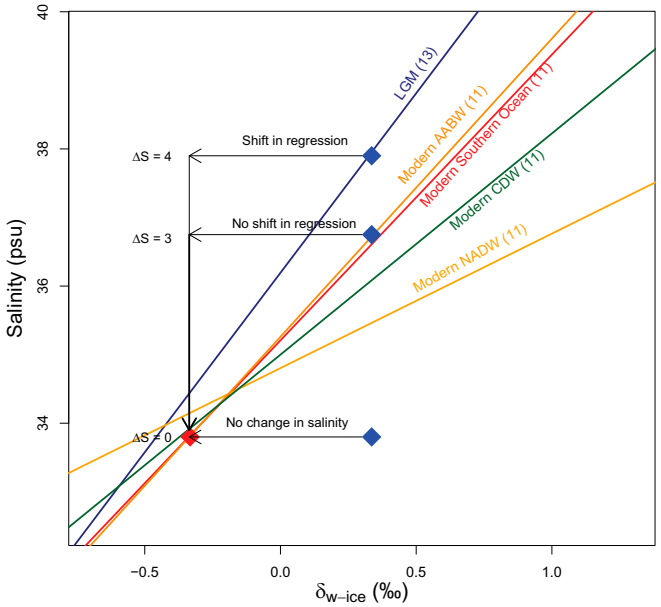

Fig. S9. Thought experiment investigating the range of deglacial salinity changes possible due to a change in the salinity–$\delta_{w\text{-}ice}$ relationship. The modern and LGM data are shown for MD07-3076Q (red and blue filled diamonds) overlain onto the salinity–$\delta_{w\text{-}ice}$ relationships for modern water masses (21), AABW, CDW, and NADW. The Holocene-LGM difference in salinity is shown for three experiments, where (*i*) there is no deglacial change in the salinity–$\delta_{w\text{-}ice}$ regression; (*ii*) there is a shift in the salinity–$\delta_{w\text{-}ice}$ regression from a salinity–$\delta_{w\text{-}ice}$ regression as estimated by Southern Ocean pore-water profiles (15) to the modern Southern Ocean salinity–$\delta_{w\text{-}ice}$ regression (21); and (*iii*) when all of the salinity change in the deep ocean can be explained by a change in the salinity–$\delta_{w\text{-}ice}$ regression.

Table S1. Age control points of GC528

Core depth, cm	^{14}C age, y before present	± Error, y	Reservoir age, y	± Error, y	Laboratory
0	2,540	30	967	110	BetaAnalytic
5.5	2,090	30	967	110	BetaAnalytic
30	4,972	45	967	110	Godwin/UB
41	6,178	39	967	110	Godwin/UB
49	7,150	30	967	110	BetaAnalytic
58	9,383	48	967	110	Godwin/UB
61	7,876	51	967	110	Godwin/UB
61	9,026	48	967	110	Godwin/UB
66	11,925	48	987	110	Godwin/UB
72	12,562	55	1,031	110	Godwin/UB
78	12,652	53	1,040	110	Godwin/UB
82	12,295	53	1,077	110	Godwin/UB
88	12,611	47	1,077	110	Godwin/UB
98	13,251	50	1,084	110	Godwin/UB
109.5	12,234	65	1,150	110	Godwin/UB
111.5	13,079	63	1,175	110	Godwin/UB
119	13,670	70	1,298	110	Godwin/UB
124	14,410	81	1,325	110	Godwin/UB
139.5	14,651	80	1,330	110	Godwin/UB
149	16,380	90	1,364	110	BetaAnalytic
199	17,340	101	1,364	110	Godwin/UB
229	17,220	70	1,364	110	BetaAnalytic
289	18,260	108	1,364	110	Godwin/UB
350	20,628	140	1,364	110	Godwin/UB
416	29,475	372	1,364	110	Godwin/UB